A computational model of a PEM fuel cell with finite vapor absorption rate

A. Vorobev, O. Zikanov [*], T. Shamim

Department of Mechanical Engineering, University of Michigan-Dearborn, 48128-1491 Dearborn, MI, USA

Received 30 November 2006; received in revised form 21 December 2006; accepted 21 December 2006
Available online 12 January 2007

Abstract

The paper presents a new computational model of non-steady operation of a PEM fuel cell. The model is based on the macroscopic hydrodynamic approach and assumptions of low humidity operation and one-dimensionality of transport processes. Its novelty and advantage in comparison with similar existing models is that it takes into account the finite-time equilibration between vapor and membrane-phase liquid water within the catalyst layers. The phenomenon is described using an additional parameter with the physical meaning of the typical reciprocal time of the equilibration. A computational parametric study is conducted to identify the effect of the finite-time equilibration on steady-state and transient operation of a PEM fuel cell.
© 2007 Elsevier B.V. All rights reserved.

Keywords: PEM fuel cell; Modeling; Water management

1. Introduction

The polymer electrolyte membrane (PEM) fuel cells are promising power sources with numerous potential and already realized applications. Although a subject of scientific scrutiny for several decades, the operation of these devices is still not fully understood. The main reason is the complexity of the underlying physical phenomena, which, in particular, concerns the interconnected processes of transport of gaseous and liquid species and phase transformation of water.

It has been long understood that the experimental approach alone is insufficient and should be complemented by theoretical and computational models, which provide needed insight into the cell operation and possibility of the cell optimization. Numerous models have been developed over the last two decades (see Refs. [1,2] for a recent review and Refs. [3–5] for further examples). The past modeling studies identified the effects, which are vitally important for the fuel cell operation and require accurate modeling. A particularly important area, which can be greatly assisted with more accurate modeling, is the water management of fuel cell. The goal of the water management is two-fold. The membrane hydration has to be maintained at

a desired level. On the other hand, condensation of excessive water into droplets within gas diffusion and catalyst layers has to be avoided since it leads to blockage of the transport of gas reactants.

In the present paper, we utilize the principles of macroscopic mass transfer to develop a model of a single fuel cell. The novelty of our approach is in the description of the transport and phase transformation of water within the catalyst layers. As opposite to almost all previous studies (the only exception [6] is discussed below), we do not assume equilibrium between the pore vapor and membrane liquid water but rather consider them as different phases equilibrating at a finite rate. Let us introduce the phenomenon and discuss it in some details.

Catalyst layers, the most complex and important parts of any fuel cell, generally consist of three phases: a solid matrix, a polymer membrane phase with attached agglomerates of liquid water, and pores filled with a gas mixture. The concentrations of liquid water retained in the agglomerates and water vapor in the pores are determined by their diffusive and convective transport and phase transition into each other. The traditional theoretical approach is to assume that the liquid and vapor phases within the catalyst layers are at equilibrium with each other described by the experimental uptake curve. The curve was originally obtained in Ref. [7] as an equilibrium relation between the average liquid water content within the membrane and the vapor concentration in the surroundings. It was mentioned in Ref. [7] that the equi-

---

* Corresponding author.
  E-mail address: zikanov@umd.umich.edu (O. Zikanov).

librium was not achieved instantly but over a prolonged period of time determined by the slow diffusion of liquid water through the membrane.

It has been long understood that the slow equilibration between the membrane water content and vapor concentration in anode and cathode has to be taken into account by any unsteady fuel cell model. This was done, for example, in the recent work [8]. The approach was, however, not followed in the description of the processes within the catalyst layers, where an equilibrium between vapor and liquid water was assumed. As it is discussed in Section 2.2 of the present paper, the assumption, although acceptable as a first approximation, is not entirely correct.

The present paper questions the validity of the equilibrium assumption applied within the catalyst layers by considering that the ionomer water forms agglomerates and, thus, not all hydrophilic elements of the ionomer are in contact with the pore vapor. The complete equilibration would occur only over the relaxation time determined by the diffusion of liquid water through the agglomerates. Moreover, the combination of the finite-rate relaxation and diffusive water transport within the agglomerates and pores may lead to absence of equilibrium even in steady-state behavior.

Addressing this issue, we incorporate the phase transition into the model of a single fuel cell and investigate the sensitivity of the cell performance to the absorption rate of vapor by ionomer in the catalyst layers. We use the approach of Ref. [6], where

a simple phenomenological model of the process was proposed and analyzed for the case of a separate cathode catalyst layer. The rate of equilibration is defined as a constant τ_γ^{-1}, where τ_γ is the typical relaxation (equilibration) time, which primarily depends on the volume fraction of the ionomer in the catalyst layer and the area of the contact surface. The upper bound of this time scale can be estimated for the cell properties used in the present study (see Table 1) as $\tau_\gamma^{max} = (m^{1/3}L_c)^2/D_{m,eff} \sim 0.5$ s. Here L_c is the thickness of the catalyst layer, m is the volume fraction of ionomer in the catalyst layer, and $D_{m,eff}$ is the effective diffusivity coefficient of the ionomer water related to the membrane diffusivity D_m via the Bruggeman correlation. The estimate should be understood as an unrealistic upper bound, since it is based on the assumption that a single agglomerate has the dimension L_c of the thickness of the catalyst layer. The actual relaxation time τ_γ is likely to be considerably, perhaps two or three orders of magnitude, smaller than τ_γ^{max}.

Since our primary interest is in the automotive applications, where the load and external conditions (temperature, air humidity, etc.) may vary with time, the focus of the investigation is on the transient regimes of the fuel cell operation. It is necessary to mention that, with few exceptions, the fuel cell models reported in the literature are limited to steady-state or quasi-steady-state solutions.

The non-steady cell operation is governed by very different time scales. It is interesting to estimate them and compare with

Table 1
Physical, electrochemical, transport properties, and geometrical parameters of the fuel cell

Quantity	Unit	Value
Atmospheric pressure, p_{atm}	Pa	101,325
Pressure of saturated vapor, p_{sat}	Pa	$\log_{10}(p_{sat}/p_{atm}) = -2.1794 + 2.953 \times 10^{-2}(T - 273.15) - 9.1837 \times 10^{-5}(T - 273.15)^2 + 1.4454 \times 10^{-7}(T - 273.15)^3$
Diffusivity of hydrogen in gas mixture, D^{H_2}	m^{2}s^{-1}	$1.1 \times 10^{-4}(T/353)^{3/2}(p_{atm}/p)$
Diffusivity of oxygen in gas mixture, D^{O_2}	m^{2}s^{-1}	$3.2 \times 10^{-4}(T/353)^{3/2}(p_{atm}/p)$
Diffusivity of vapor in gas mixture, D^{H_2O}	m^2 s^{-1}	$7.35 \times 10^{-5}(T/353)^{3/2}(p_{atm}/p)$
Gas viscosity, μ	kg (m s)$^{-1}$	$9.88 \times 10^{-6}C^{H_2} + 1.22 \times 10^{-5}C^{H_2O} + 2.3 \times 10^{-5}C^{O_2} + 2.01 \times 10^{-5}C^{N_2}$
Open circuit potential, V_0	V	$1.23 - 9 \times 10^{-4}(T - 298)$
Membrane diffusivity, D_m	m^2 s^{-1}	$\begin{cases} 3.1 \times 10^{-7}\lambda(e^{0.28\lambda} - 1)e^{-2346/T}, \lambda \le 3 \\ 4.17 \times 10^{-8}\lambda(1 + 161e^{-\lambda})e^{-2346/T}, \lambda > 3 \end{cases}$
Ionic conductivity of the membrane, κ	A (V m)$^{-1}$	$(0.5139\lambda - 0.326)\exp[1268((1/303) - (1/T))]$
Electro-osmotic drag coefficient, n_d		1.0 for $\lambda \le 14$
Exchange current densities at the anode and cathode sides × reaction surface area, j_{ref}^a and j_{ref}^c	A m^{-3}	10^9 and 10^4
Reference hydrogen and oxygen, concentrations, $C_{ref}^{H_2}$ and $C_{ref}^{O_2}$	mol m^{-3}	40
Transfer coefficients at the anode and cathode sides, $\alpha_a + \alpha_c$ and α_c		2 and 1
Dry membrane density, ρ_{dry}	kg m^{-3}	1980
Equivalent weight of ionomer, EW	kg mol^{-1}	1.1
Porosity of the anode, ϵ		0.6
Porosity of the catalyst layer, ϵ		0.4
Volume fraction of ionomer in catalyst layers, m		0.26
Permeability of the anode and cathode, K	m^2	10^{-12}
Permeability of the catalyst layers, K	m^2	10^{-15}
Pressure at the inlet and outlet ends, p_0	Pa	$2p_{atm}$
Thickness of anode and cathode, L_1 and L_5	m	3×10^{-4}
Thickness of the anodic and cathodic catalyst layers, L_2 and L_4	m	10^{-5}
Thickness of the membrane, L_3	m	5.1×10^{-5}

All data are from Refs. [10,11].

the relaxation time introduced above. The first is the typical diffusion time of the reactant gases through anode and cathode, which can be estimated as $\tau_g = L_g^2/D_{g,eff}$, where L_g is the thickness of the anode or cathode gas diffusion layer and $D_{g,eff}$ is the effective diffusion coefficient of gaseous species. Typically, $\tau_g = 0.001 - 0.05$ s. The second time scale is related to the membrane absorption (desorption) of water. The process is characterized by a much larger diffusive time scale, which can be estimated as $\tau_m = L_m^2/D_m$, where L_m and D_m are the membrane thickness and diffusion coefficient, and is typically equal to 1–10 s.

2. Model

A fuel cell consists of porous anode and cathode diffusive layers, membrane, and two catalyst layers of small but finite thickness. Considering the focus of the present work, the model does not include the anode and cathode gas channels, and the boundary conditions are applied directly at the outer borders of the anode and cathode.

The mathematical model closely follows the model used in Ref. [2], with the major difference made in consideration of the catalyst layers. Low humidity regime of the cell operation is considered. The diffusion layers are assumed to have no liquid droplets. The vapor penetrating into the fuel cell at the anode and cathode sides is to be under partial pressure that is less than the saturated value, so no condensation occurs in these layers. The membrane (including the membrane phase of the catalyst) is filled with liquid water, and the phase transition between liquid water and vapor can occur at the surface of the membrane phase. Under the conditions of low humidity operation, the main task of water management is to prevent the membrane dehydration.

The low humidity assumption does not impose any serious limits on the scope of this investigation. It was experimentally shown in Ref. [9] that the fuel cell can be successfully utilized at low humidification levels without using external humidification. Although smaller efficiency rates are attained under such conditions, there are also advantages of avoiding the use of the external humidifiers, such as reduction in the cell cost, mass, and volume. At present, the low humidity operation is considered to be promising for small portable, including automotive, applications.

For the sake of simplicity, a one-dimensional, transient approach is taken, with all fields being functions of the coordinate x across the cell and time t. The model can be easily generalized to two and three dimensions in future studies. Temperature of the cell is assumed to be constant and equal to $80\,°C$.

In the following subsections, we formulate the governing equations and boundary conditions separately for each part of the fuel cell. The behavior of the gas mixture within the porous media is governed by the mass balance for each species and the balance of total momentum. The distribution of the membrane water content is determined by the equation for the balance of mass. The values of the physical quantities used in the simulations are summarized in Table 1.

2.1. Anode

Anode is modeled as a porous medium filled with the gas mixture which contains hydrogen, water vapor, and sometimes nitrogen and other non-reacting gases. In the simulations presented below, the transport of hydrogen and vapor is resolved directly, while the nitrogen concentration is found from the mass balance conditions. The mixture is transported through the porous medium by diffusive and convective mechanisms. The ideal gas model is adopted for the mixture.

The mass balance is expressed by the continuity equation

$$\epsilon \frac{\partial \rho}{\partial t} + \frac{\partial}{\partial x}(\rho u) = 0. \tag{1}$$

Here ϵ is the porosity of the matrix, u the filtration velocity and ρ the density of the gas mixture, which is defined through the molar concentrations and molar weights of components as

$$\rho = M^{H_2}C^{H_2} + M^{H_2O}C^{H_2O} + M^{N_2}C^{N_2}. \tag{2}$$

The permeability coefficients of the electrodes are very small, so the conservation of momentum may be described by the Darcy law

$$\frac{\partial p}{\partial x} = -\frac{\mu}{K}u. \tag{3}$$

Here, p is the gas mixture pressure and K is the permeability of the porous media.

Equations for species conservation are

$$\epsilon \frac{\partial}{\partial t}C^{H_2} + \frac{\partial}{\partial x}(uC^{H_2}) = \frac{\partial}{\partial x}\left(D_{eff}^{H_2}\frac{\partial}{\partial x}C^{H_2}\right), \tag{4}$$

$$\epsilon \frac{\partial}{\partial t}C^{H_2O} + \frac{\partial}{\partial x}(uC^{H_2O}) = \frac{\partial}{\partial x}\left(D_{eff}^{H_2O}\frac{\partial}{\partial x}C^{H_2O}\right). \tag{5}$$

The Bruggeman correlation is applied in order to find the effective diffusion coefficients

$$D_{eff}^{H_2} = \epsilon^{1.5}D^{H_2}, \qquad D_{eff}^{H_2O} = \epsilon^{1.5}D^{H_2O}. \tag{6}$$

Equation of state reads

$$p = RT(C^{H_2} + C^{H_2O} + C^{N_2}), \tag{7}$$

where R is the universal gas constant and T is the constant temperature of the cell.

At the outer (inlet) boundary of the anode layer, the concentrations of hydrogen and vapor (humidity), i.e. C^{H_2} and C^{H_2O}, as well as pressure p are assumed to be known. The concentration of nitrogen can be determined from the equation of state (7).

At the boundary separating the anode and anodic catalyst layer, continuity of hydrogen and vapor concentrations C^{H_2} and C^{H_2O} and continuity of their fluxes $D_{eff}^{H_2}\partial C^{H_2}/\partial x$, $D_{eff}^{H_2O}\partial C^{H_2O}/\partial x$ are assumed. Continuity of pressure p and mass flux ρu is also required.

2.2. Anodic catalyst layer

The material of the catalyst layer is a fusion of two fractions: a porous matrix filled with the gas mixture and the membrane,

where liquid water exists in the form of agglomerates. In the present work, both fractions are assumed to be homogeneously distributed over the thickness of the catalyst layer. The layer is considered as a porous medium with the pores formed by the solid matrix and water agglomerates. The porosity and permeability of the layer are constants, the values of which are reduced in comparison to the characteristics of the anode in order to account for the fraction occupied by the membrane phase. The transport within the catalyst layer is governed by the equations of the gas mixture filling the pores. Convection within the ionomer, as well as diffusion of gas components through liquid water are considered negligible.

It is assumed that hydrogen oxidation reaction ($H_2 - 2H^+ = 2e^-$) occurs in the pores. Protons are then diffused though the membrane phase of the catalyst layer and the membrane to the cathodic catalyst layer.

Traditionally, the membrane liquid water content (hydration) is characterized by the quantity λ which is defined as the number of water molecules per sulfonic-acid group (SO_3^-) (see, e.g., [7]). The liquid water content can be at equilibrium with the surrounding vapor at arbitrary vapor concentration. The situation is principally different from the simple evaporation–condensation process due to the additional internal energy of the membrane active centers that keeps the water molecules in the agglomerates. The equilibrium is defined by the uptake curve, traditionally expressed as a relation between the membrane hydration λ and the vapor activity $a \equiv RTC^{H_2O}/p_{sat}$, where p_{sat} is the saturated vapor pressure. According to Ref. [7], the uptake curve can be approximated as

$$\lambda_e = \begin{cases} 0.0043 + 17.81a - 39.85a^2 + 36.0a^3, & \text{for } 0 < a \leq 1 \\ 14 + 1.4(a - 1), & \text{for } 1 < a \leq 3. \end{cases} \quad (8)$$

Here the subscript e stands for the equilibrium.

In earlier models that considered water transport within the catalyst layer, instant equilibrium (8) between the vapor and ionomer liquid was assumed. This assumption, albeit suitable as a first approximation, is not strictly correct. The membrane liquid water in the catalyst layer forms large agglomerates. Only a small portion of the ionomer adjacent to the agglomerate surfaces is in direct contact with the pore gas. Any variation of the vapor activity is followed by immediate corresponding change of the liquid water content in the surface region but takes some finite time to diffuse into the interior. As a result, the equilibration is achieved only after certain typical time, which was estimated in Section 1 as 10^{-3} to 10^{-1} s. Furthermore, there can be steady-states characterized by the absence of equilibrium between the vapor and liquid water. Finite rate equilibration is offset in such states by the spatial diffusion of water.

It can also be mentioned that the instant equilibrium approach leads to an inconsistency in formulation of the boundary conditions at the catalyst borders. At the boundary between the anode and catalyst layer, vapor passes freely, whereas liquid water is trapped in the membrane phase and does not penetrate into the anode. At the opposite boundary, the assumption is made that the vapor does not diffuse into the membrane, while the liquid water

of the catalyst membrane phase does. These boundary conditions cannot be modeled correctly if one-to-one correspondence between the vapor concentration and water content of membrane phase is assumed.

The present analysis incorporates a more realistic description of the water absorption and desorption by the membrane phase. The transition between the vapor and liquid water is described with the help of a phenomenological model proposed in Ref. [6] and conceptually analogous to the common evaporation–condensation model. The rate of change of concentration of liquid water and vapor is assumed to be proportional to the deviation of the actual hydration λ from the equilibrium hydration λ_e given by (8). The phenomenological coefficient of proportionality is a constant equal to the typical reciprocal equilibration time τ_γ.

The governing equations in the gas pores include the continuity equation for the gas mixture, Darcy law (conservation of momentum), and the diffusion equations for hydrogen and vapor

$$\epsilon \frac{\partial \rho}{\partial t} + \frac{\partial}{\partial x}(\rho u) = -M^{H_2} \frac{1}{2F} j - M^{H_2O} \gamma^* (p_m \lambda_e - C_\lambda^{H_2O}), \quad (9)$$

$$\frac{\partial p}{\partial x} = -\frac{\mu}{K} u, \quad (10)$$

$$\epsilon \frac{\partial}{\partial t} C^{H_2} + \frac{\partial}{\partial x}(u C^{H_2}) = \frac{\partial}{\partial x}\left(D_{eff}^{H_2} \frac{\partial}{\partial x} C^{H_2}\right) - \frac{1}{2F} j, \quad (11)$$

$$\epsilon \frac{\partial}{\partial t} C^{H_2O} + \frac{\partial}{\partial x}(u C^{H_2O})$$
$$= \frac{\partial}{\partial x}\left(D_{eff}^{H_2O} \frac{\partial}{\partial x} C^{H_2O}\right) - \gamma^* (p_m \lambda_e - C_\lambda^{H_2O}). \quad (12)$$

Here, F is the Faraday constant and j is the transfer current of the hydrogen oxidation reaction discussed below.

The membrane phase is assumed to be impermeable to gases. The transport of liquid water is given by the diffusion equation

$$m \frac{\partial}{\partial t} C_\lambda^{H_2O} = \frac{\partial}{\partial x}\left(D_{m,eff}^{H_2O} \frac{\partial}{\partial x} C_\lambda^{H_2O}\right) - \frac{n_d}{F} j$$
$$+ \gamma^* (p_m \lambda_e - C_\lambda^{H_2O}). \quad (13)$$

The water transport by the electro-osmotic drag of water molecules by migrating protons is included in Eq. (13) with the assumption that electro-osmotic coefficient n_d is constant [12].

Eq. (13), which did not appear in previous models, is required in our model since the equilibrium between the liquid water and vapor is not imposed. In addition to the terms describing the diffusive and convective transport and the consumption of hydrogen in the electrochemical reaction, the Eqs. (9)–(13) contain new terms describing the absorption or desorption of vapor by the membrane phase. $C^{H_2O} = p_{sat}a$ is the molar vapor concentration, where a is the water activity. $C_\lambda^{H_2O} = p_m \lambda$ is the quantity characterizing the water content of membrane phase ($p_m \equiv \rho_{dry}/EW$, where ρ_{dry} is the density of the dry membrane and EW is the equivalent weight defined as the weight of the membrane per mole of sulfonic acid group). $\gamma^* \equiv \tau_\gamma^{-1}$ is the proposed phenomenological parameter. In the following, we will

use the non-dimensional relaxation parameter $\gamma \equiv \tau_g \gamma^*$, where τ_g is the typical gas diffusion time, which is estimated as $L^2/D_{\mathrm{eff}}^{\mathrm{H}_2}$ using the total thickness of the cell and the effective diffusivity of hydrogen at $p = p_{\mathrm{atm}}$. The parameter γ is varied between 100 (almost immediate equilibrium) and 0.1 (very slow equilibration). This corresponds to the range $11.4 \leq \gamma^* \leq 1.14 \times 10^4 \mathrm{s}^{-1}$ and the dimensional relaxation time τ_γ between 8.8×10^{-5} and 8.8×10^{-2} s.

All diffusion coefficients in (9)–(13) are modified via the Bruggeman correlation as follows

$$D_{\mathrm{eff}}^{\mathrm{H}_2} = \epsilon^{1.5} D^{\mathrm{H}_2}, \qquad D_{\mathrm{eff}}^{\mathrm{H}_2\mathrm{O}} = \epsilon^{1.5} D^{\mathrm{H}_2\mathrm{O}},$$
$$D_{\mathrm{m,eff}}^{\mathrm{H}_2\mathrm{O}} = m^{1.5} D_{\mathrm{m}}, \tag{14}$$

where m is the volume fraction taken by the ionomer in the catalyst layer.

The model also includes the equation of state and definition of the density of the gas mixture equivalent to (7) and (2).

Additional equations are needed to describe the electric current within the catalyst layer. We assume that the membrane is impermeable to the electrons, while the solid matrix of the anode and cathode is ideally conductive. These standard assumptions allow us to model the anode and cathode as equipotential surfaces

$$\Phi_s = 0 \text{ on the anode}, \quad \Phi_s = V_{\mathrm{cell}} \text{ on the cathode.} \tag{15}$$

Here, Φ_s is the potential of the electronic phase. In all of the following equations, Φ stands for the potential of the ionic phase.

The transfer current, $j = \partial i/\partial x$, is given by the Butler–Volmer equation [2], which is used in its linearized form

$$j = j_a (C^{\mathrm{H}_2})^{1/2} \Phi, \quad j_a \equiv j_{\mathrm{ref}}^a (C_{\mathrm{ref}}^{\mathrm{H}_2})^{-1/2} \frac{\alpha_a + \alpha_c}{RT} F. \tag{16}$$

The material properties j_{ref}^a, $C_{\mathrm{ref}}^{\mathrm{H}_2}$, α_a, and α_c are given in Table 1.

The distribution of potential within the catalyst layer is defined by the equation for charge conservation:

$$\frac{\partial}{\partial x}\left(\kappa_{\mathrm{eff}} \frac{\partial \Phi}{\partial x}\right) + j = 0. \tag{17}$$

Here, κ_{eff} is the conductivity of the membrane phase of the catalyst layer, related to the membrane ionic conductivity κ (see Table 1) via the Bruggeman correlation $\kappa_{\mathrm{eff}} = m^{1.5}\kappa$.

The boundary between the anode and anodic catalyst layer was considered in Section 2.1. The additional boundary conditions for the fields $C_\lambda^{\mathrm{H}_2\mathrm{O}}$ and Φ are, respectively, that of zero flux of liquid water $\partial C_\lambda^{\mathrm{H}_2\mathrm{O}}/\partial x = 0$ and zero proton current $\partial \Phi/\partial x = 0$.

The boundary conditions at the boundary between the anodic catalyst layer and the membrane are based on the assumption that the gases do not permeate the membrane. This means zero flux of hydrogen and vapor $\partial C^{\mathrm{H}_2}/\partial x = 0$, $\partial C^{\mathrm{H}_2\mathrm{O}}/\partial x = 0$ and zero mixture velocity $u = 0$ (or, equivalently, $\partial p/\partial x = 0$). The liquid water content $C_\lambda^{\mathrm{H}_2\mathrm{O}}$ and its flux $D_{\mathrm{m,eff}}^{\mathrm{H}_2\mathrm{O}}\partial C_\lambda^{\mathrm{H}_2\mathrm{O}}/\partial x$ are assumed to be continuous. Furthermore, continuity is required for the potential Φ and the proton current $\kappa \partial \Phi/\partial x$.

2.3. Membrane

The membrane is completely filled with liquid water (presence of dissolved gases is neglected). The water transport is determined by diffusion and electro-osmotic drag. The latter mechanism is defined by the term proportional to $-(\partial n_{\mathrm{d}} i)/(\partial x)$, where i is the current density and n_{d} is the electro-osmotic coefficient. As reported in Ref. [12], n_{d} is close to 1.0 in the range of water content $\lambda \leq 14$ considered in the present work. Since there is no chemical reactions within the membrane, i is constant there. The last two facts mean that the electro-osmotic drag, although present in the membrane, does not change the internal water distribution. Owing to the osmotic drag, the water molecules are transported from the anodic catalyst layer to the cathodic one, which only affects the water content of the catalyst layers.

The membrane is assumed to be almost impermeable for gases (the actual permeability is estimated as $K \sim 10^{-18}$ to 10^{-20} m^2), i.e., the filtration velocity u is assumed to be zero.

The equation for diffusion of liquid water is

$$\frac{\partial}{\partial t} C_\lambda^{\mathrm{H}_2\mathrm{O}} = \frac{\partial}{\partial x}\left(D_{\mathrm{m}} \frac{\partial}{\partial x} C_\lambda^{\mathrm{H}_2\mathrm{O}}\right). \tag{18}$$

The transport of protons in the membrane is described by the equation for charge conservation:

$$\frac{\partial}{\partial x}\left(\kappa \frac{\partial \Phi}{\partial x}\right) = 0. \tag{19}$$

The boundary conditions at the anodic border of the membrane were discussed in Section 2.2. The boundary conditions at the cathode side are analogous. The only difference is that the flux of oxygen (instead of hydrogen) is assumed to be zero.

2.4. Cathodic catalyst layer

The gas species behavior in the cathodic catalyst layer is described by the model similar to that for the anode side. The difference is in the composition of the gas mixture (oxygen, nitrogen and water vapor) and in the type of chemical reaction, which is now the reduction of oxygen ($2\mathrm{H}_2\mathrm{O} - \mathrm{O}_2 - 4\mathrm{H}^+ = 4\mathrm{e}^-$).

The equations of continuity, Darcy law, species conservation, and the liquid water transport are

$$\epsilon \frac{\partial \rho}{\partial t} + \frac{\partial}{\partial x}(\rho u) = -M^{\mathrm{O}_2} \frac{1}{4F} j - M^{\mathrm{H}_2\mathrm{O}} \gamma^* (p_{\mathrm{m}}\lambda_{\mathrm{e}} - C_\lambda^{\mathrm{H}_2\mathrm{O}}), \tag{20}$$

$$\frac{\partial p}{\partial x} = -\frac{\mu}{K} u, \tag{21}$$

$$\epsilon \frac{\partial}{\partial t} C^{\mathrm{O}_2} + \frac{\partial}{\partial x}(u C^{\mathrm{O}_2}) = \frac{\partial}{\partial x}\left(D_{\mathrm{eff}}^{\mathrm{O}_2} \frac{\partial}{\partial x} C^{\mathrm{O}_2}\right) - \frac{1}{4F} j, \tag{22}$$

$$\epsilon \frac{\partial}{\partial t} C^{\mathrm{H}_2\mathrm{O}} + \frac{\partial}{\partial x}(u C^{\mathrm{H}_2\mathrm{O}})$$
$$= \frac{\partial}{\partial x}\left(D_{\mathrm{eff}}^{\mathrm{H}_2\mathrm{O}} \frac{\partial}{\partial x} C^{\mathrm{H}_2\mathrm{O}}\right) - \gamma^* (p_{\mathrm{m}}\lambda_{\mathrm{e}} - C_\lambda^{\mathrm{H}_2\mathrm{O}}), \tag{23}$$

$$\frac{\partial}{\partial t} C_\lambda^{H_2O} = \frac{\partial}{\partial x} \left(D_{m,eff}^{H_2O} \frac{\partial}{\partial x} C_\lambda^{H_2O} \right) - \frac{1}{F} \left(\frac{1}{2} + n_d \right) j$$
$$+ \gamma^* (p_m \lambda_e - C_\lambda^{H_2O}). \tag{24}$$

As in the anodic catalyst layer, a transport equation is used to describe the liquid water transport and source terms are added to account for the transition between liquid water and vapor.

The equation of state is

$$p = RT(C^{O_2} + C^{H_2O} + C^{N_2}). \tag{25}$$

The density of the gas mixture is defined as

$$\rho = M^{O_2} C^{O_2} + M^{H_2O} C^{H_2O} + M^{N_2} C^{N_2}. \tag{26}$$

The distribution of potential within the catalyst layer is described by the equation of conservation of charge

$$\frac{\partial}{\partial x} \left(\kappa_{eff} \frac{\partial \Phi}{\partial x} \right) + j = 0. \tag{27}$$

The transfer current in Eqs. (20)–(27) is given by the Butler–Volmer equation

$$j = j_c C^{O_2} \exp(\alpha \Phi), \tag{28}$$

where the following dimensional parameters are introduced (see Table 1 for the physical properties)

$$j_c = j_{ref}^c (C_{ref}^{O_2})^{-1} \exp \left(\frac{\alpha_c F}{RT} (V_{cell} - V_0) \right), \quad \alpha = \frac{\alpha_c F}{RT}. \tag{29}$$

The Bruggeman correlation (14) is used to find the effective diffusivity and ionic conductivity coefficients.

The boundary conditions at the surface between the membrane and the cathode catalyst layer include zero fluxes of oxygen and water vapor $\partial C^{O_2}/\partial x = 0$, $\partial C^{H_2O}/\partial x = 0$, zero gas mixture velocity $u = 0$, and continuities of the liquid water content $C_\lambda^{H_2O}$, its flux $D_{m,eff}^{H_2O} \partial C_\lambda^{H_2O}/\partial x$, ionic potential Φ, and current $\kappa_{eff} \partial \Phi/\partial x$.

The conditions imposed at the boundary between the catalyst layer and the cathode, are continuities of concentrations of gas species C^{O_2}, C^{H_2O}, their fluxes $D_{eff}^{O_2} \partial C^{O_2}/\partial x$, $D_{eff}^{H_2O} \partial C^{H_2O}/\partial x$, and the total mass flux ρu. We also require zero fluxes of liquid water $\partial C_\lambda^{H_2O}/\partial x = 0$ and ionic current $\partial \Phi/\partial x = 0$.

2.5. Cathode

The equations and the boundary conditions describing the mass balance within the cathode are identical to those for the anode and can be easily obtained by substitution of the quantities for the hydrogen by the corresponding quantities for oxygen.

2.6. Method of solution

The problem is simplified by eliminating the filtration velocity u from consideration through substitution of the Darcy law into the continuity and species conservation equations and boundary conditions. The resulting system is solved by the finite-difference method. The spatial discretization is achieved by applying the second-order central discretization formulas to all spatial derivative terms written in the conservation form. The time integration is based on the explicit Runge–Kutta method of the second order.

Each time step includes the actual time integration of the evolution equations and the solution of the boundary-value problem for the ionic potential. At the first substep, the time integration is performed, which results in new concentration fields satisfying the balance equations and boundary conditions. At the second sub-step, the updated species concentrations are used to find the distribution of potential at the new time level. For this purpose, the charge conservation equation is integrated over the catalyst layers and the membrane with no-flux boundary conditions at the outer boundaries. Solution of the boundary-value problem is determined by the shooting algorithm. Determining the potential field in this fashion is computationally intensive. The field, however, varies significantly only when the membrane water content changes. One also has to take into account that the time step used in the present calculations is very small, several orders of magnitude smaller than the typical time of water diffusion through the membrane. It is, therefore, unnecessary to adjust the potential at every time step. We found that, in the cases considered in the present paper, adjustment after every 1000 time steps is sufficient for accurate computation. The coefficients of diffusivity, conductivity, and viscosity are renewed at the beginning of each time-step.

The finite-difference grid is uniform within each sub-domain of the cell (anode, cathode, membrane, and catalyst layers). The grid steps are different in different sub-domains. We conducted a series of computations with numerical grids consisting of 10, 20, and 30 points in each subdomain. Numerical convergence was clearly observed for both transient and steady-state solutions. The solution fields obtained with 20 and 30 points in each subdomain were almost indistinguishable, which indicated the accuracy and acceptability of a 20-point grid. All the results presented below in this paper were obtained using this grid. The time step was constant and equal to 4.4×10^{-9} s, which constitutes $5 \times 10^{-7} \tau_g$.

As initial conditions, the uniform distributions of concentration of hydrogen in the anode and of oxygen in the cathode, of vapor and nitrogen in both parts, as well as uniform pressure throughout the entire fuel cell were specified. The water content in the membrane was assumed to be initially in equilibrium with the vapor concentration. The cell was assumed to be fed by pure hydrogen at the anode side and by air ($C_{in}^{N_2}/C_{in}^{O_2} = 0.79/0.21$ on the cathode side).

3. Numerical results

3.1. Model validation

The model was validated by comparing the steady-state results with the results of three-dimensional model [11] chosen because of the closest agreement with our model in regard of the physical effects taken into account and availability of a detailed description of the simulation parameters. The assumption of the uptake curve equilibrium between the vapor and liquid
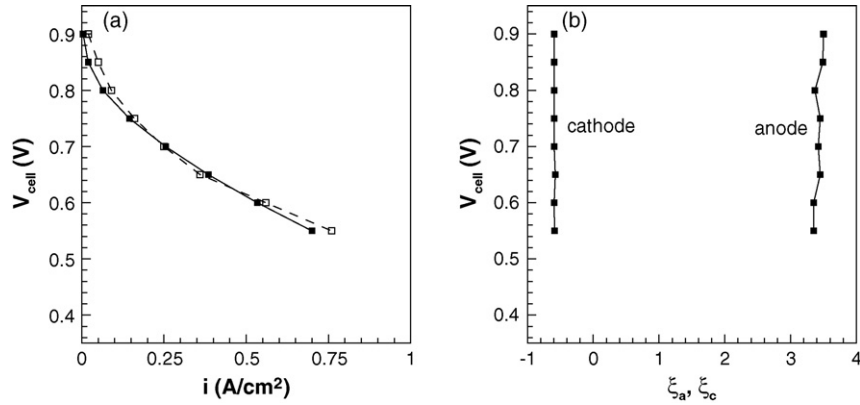
Fig. 1. (a) Comparison of polarization curves. Solid line represents the results obtained with the present model, the dashed line corresponds to the model [11]. (b) Stoichiometric coefficients defined by (30). External conditions correspond to 50% humidity of the fuel and air. $\gamma = 100$.

water in the catalyst layers was made in Ref. [11]. As a nearest approximation achievable in the framework of our model, the simulations used for comparison were performed in the limit of fast equilibration (large relaxation parameter γ). We found that $\gamma = 100$ was sufficiently large to represent the asymptotic limit $\gamma \to \infty$, the solution being insensitive to further increase of γ.

Fig. 1a shows the comparison of the polarization curves. The curves are in good qualitative agreement, although there are some quantitative differences. Such a discrepancy can be explained as follows. First, there is an inherent difference between 3D and 1D models. It was shown in Ref. [11] that the multi-dimensional effects influence the cell's performance. The distributions of concentrations and other fields vary significantly along the cell. Any 1D model can only be considered as an approximation representing the bulk properties.

Further explanation is related to the difference in the specification of the external boundary conditions. In Ref. [11] and many other models, the boundary conditions are imposed at the inlets and exits of the gas channels. The gas species distributions were found to vary significantly along the channels. In our model the channels are not included and the boundary conditions are imposed at the outer surfaces of the anode and cathode diffuser layers. This does not allow us to reproduce the conditions of earlier simulations exactly. For example, the curve corresponding to the results of Ref. [11] in Fig. 1a was obtained at 50% and 0% humidity at the inlets to the anode and cathode channels, respectively. Actual humidity at the channel/diffuser boundaries varied significantly. Figs. 5 and 7 of Ref. [11] show the humidity in the anode channel varying between approximately 25% and 75% and humidity in the cathode channel growing from 0% to about 100%. The distributions corresponding to different points of the polarization curve also differ from each other. In order to imitate the conditions of Ref. [11], we assumed 50% humidity at both the anode and cathode outer boundaries.

Another aspect also related to the specification of the boundary conditions is that, in Ref. [11] and some other models, the inlet velocities of each species were specified by the values of the stoichiometric coefficients, defined as

$$\xi_a = \frac{2 C_a^{H_2} u_a F}{i}, \qquad \xi_c = \frac{4 C_c^{O_2} u_c F}{i}. \tag{30}$$

Here u_a, u_c are the inlet velocities (the sign is taken so that positive u_a or u_c correspond to a flow into the cell) and $C_a^{H_2}$, $C_c^{O_2}$ are the hydrogen and oxygen concentrations at the anode and cathode side, respectively. These coefficients define the ratios between the amounts of each reactant coming into the cell to the amounts of reactant consumed inside. These coefficients are always assumed to be more than 1 (e.g., $\xi_a = 1.2$ or 2 and $\xi_c = 2$ in Ref. [11]). The present model, as mentioned earlier, does not include the gas channels. The model assumes that the flow of the reactant gases into the anode and cathode layers is induced by their consumption inside and, so, the entire amounts entering the cell are burnt inside. The values of pressure and species concentrations are specified at the surfaces of the diffuser layers as input parameters. The values are taken to be the same at any voltage and current density and, thus, are different from the current-dependent values that would be obtained in simulations including the gas channels and using the boundary conditions on the stoichiometric coefficients (30).

As an illustration of our approach to formulation of boundary conditions, the stoichiometric coefficients estimated on the basis of the obtained solution are shown in Fig. 1b. The figure depicts that the coefficients are only weakly dependent on the cell voltage or current densities, which means the values of the inlet velocities vary proportionally to the values of the current density. It is worthwhile to point out that ξ_a and ξ_c represent only convective transport into the diffusive layers. The analogous coefficients representing the full (convective plus diffusive) transport are always 1 in our model. The data in Fig. 1b, thus, provide non-trivial information on the relative significance of the two transport mechanisms. ξ_a exceeds 1, which means that the diffusive transport is negative (out of the cell). On the cathode side, ξ_c is negative corresponding to the convective transport of oxygen out of the cell. The net positive transport into the cell is provided by the strong diffusive flux caused by the negative gradient of the oxygen concentration.

3.2. Steady-state regimes

The steady-state solution obtained for the point $V_{cell} = 0.65 \, V$ of the polarization curve is illustrated in Fig. 2. The
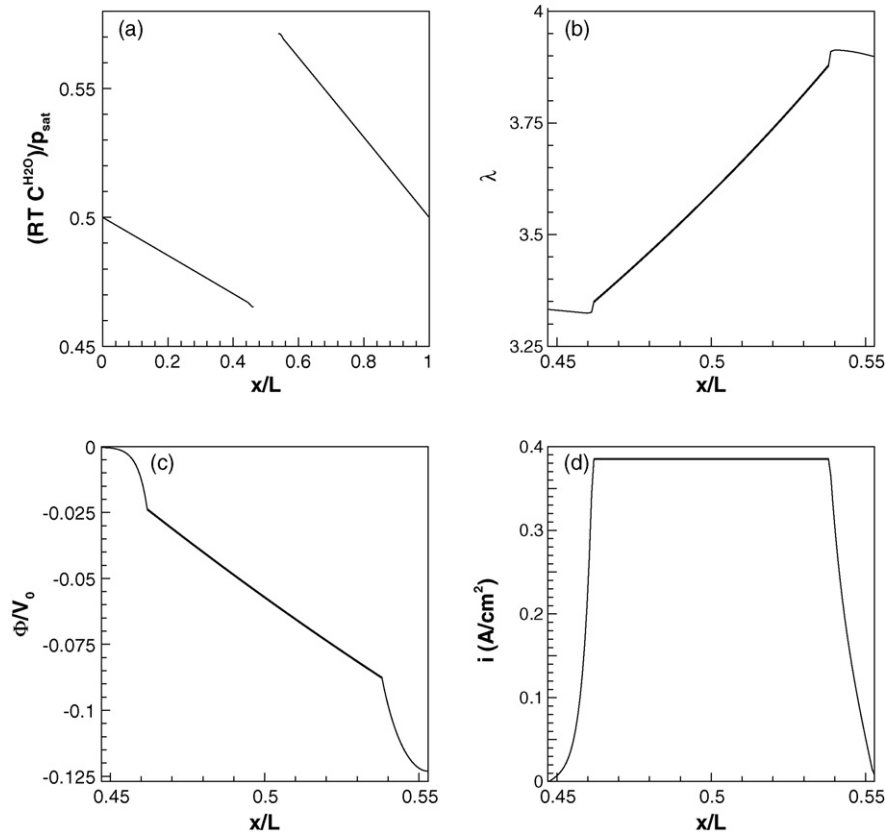
Fig. 2. Steady state solutions at $V_{cell} = 0.65\,V$, 50% humidity of the fuel and air, $\gamma = 100$. (a) Vapor concentration in anode, cathode, and catalyst layers; (b–d) liquid water content, ionic potential (in units of open circuit potential V_0), and current density in catalyst layers and membrane. The membrane domain is indicated by bold lines.

distributions of vapor concentration C^{H_2O}, membrane water content λ, ionic potential Φ, and current density i are shown. The profiles of gas species concentrations and pressure (not shown) demonstrate very small variations (less than 5%) within the cell.

Many features of the distributions shown in Fig. 2 are typical for 1D simulations. The humidity profiles in Fig. 2a form as a result of the balance between the electrochemical production of water within the cathode catalyst layer, osmotic drag, and the diffusive and convective transport in the presence of constant humidity conditions at the outer surfaces of anode and cathode. The water content λ within the membrane shows almost linear growth from the anode to cathode side. Such a distribution, albeit similar to the results of earlier one-dimensional models, is in a disagreement with certain experiments, such as [13]. It has to be stressed that the linearity was not presumed by our model. The distribution of λ was obtained as a solution of the transport Eq. (18) with a λ-dependent diffusivity coefficient D_m (see Table 1). The experimental distribution could be affected by other factors not taken into account by the model. The most significant among them are the possible variability of the osmotic drag coefficient n_d [13], two- and three-dimensionality effects [5], and the pressure gradient [3]. We note that, despite possible inaccuracies in representing the space distributions, our model provides the volume-averaged values of λ, which are very close to the results of earlier works, such as 3D computations of Ref. [11].

The ionic potential and current density are shown in Fig. 2c and d. The rate of ohmic voltage drop is almost constant within the membrane. The change of ionic conductivity κ due to the variation of liquid content λ is insignificantly small to cause any appreciable effect on the Φ-profile. Within the catalyst layer, $\kappa_{eff}(= m^{1.5}\kappa)$ decreases sharply, which results in increased ohmic losses in the regions near the membrane.

A novel feature of the present model is that vapor and liquid water are considered separately from each other in the catalyst layers and are not required to be in equilibrium with each other. This opens an interesting question of the effect of the relaxation parameter γ on the steady-state behavior of the cell. To answer it, we conducted simulations at $V_{cell} = 0.7\,V$ and with γ varying between 0.1 and 100. The results are illustrated in Fig. 3, which shows that the entire distributions of vapor concentration C^{H_2O} and liquid water content λ change significantly with γ. Computations performed for other points of the polarization curve showed that the effect becomes even more pronounced at larger current density.

Fig. 3a shows that the value of γ affects the vapor concentration C^{H_2O} in the catalyst layers. A decrease of γ (increase of the relaxation time τ_γ) leads to the growth of C^{H_2O} in the anode catalyst layer and a decrease in the cathode catalyst layer. The overall effect is that of reduced gradient of vapor concentration across the anode and cathode. The impact of changing γ on the liquid water content is also significant (see Fig. 3b). A decrease
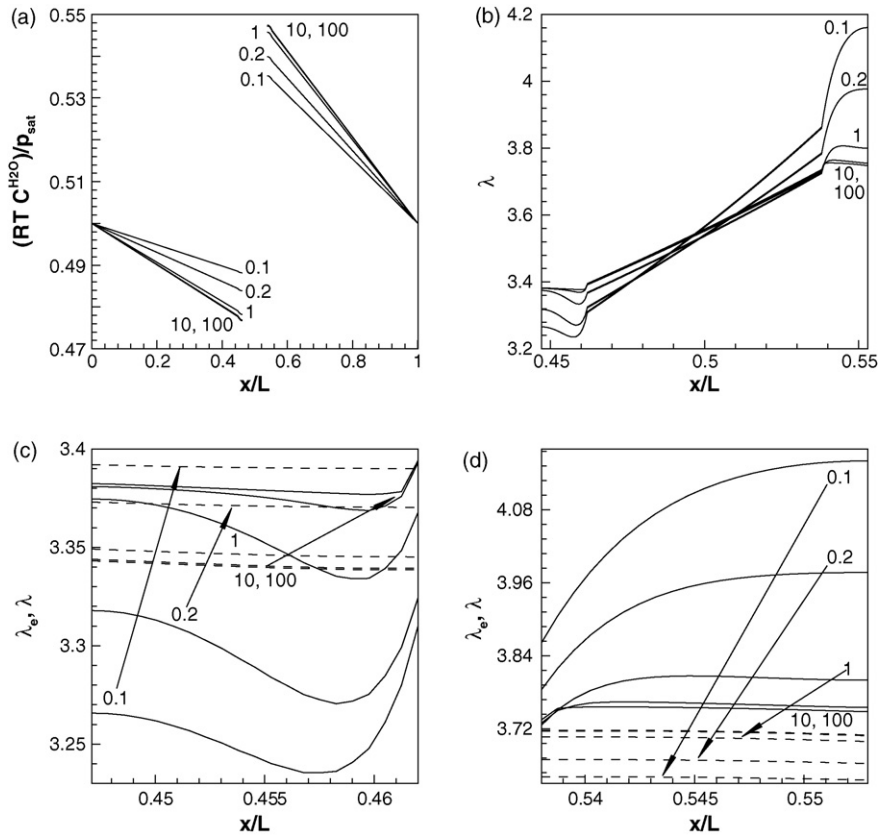
Fig. 3. Steady state solutions obtained for different values of γ at $V_{cell} = 0.7$ and 50% humidity of the fuel and air. (a) Vapor concentration in anode and cathode; (b) liquid water content in the catalyst layers and membrane; (c and d) comparison between actual water content λ (solid lines) and equilibrium water content λ_e (dashed lines) corresponding to the computed vapor concentration.

of γ results in a stronger variation of λ across the membrane. In the catalyst layers, the distributions of λ form clearly visible zones of boundary-layer behavior near the catalyst-membrane surfaces. Widths of the zones and the amplitudes of variation of λ within them grow with decreasing γ. The zones can be detected in our model since the assumption of the uptake curve equilibrium between C^{H_2O} and λ is not made. It can be deduced that using this assumption would inevitably lead to non-physical behavior at the membrane-catalyst border, either violation of the no-flux condition for C^{H_2O} or discontinuity of λ.

Fig. 3c and d show comparison between the distribution of λ across the catalyst layers and the equilibrium distributions λ_e calculated on the basis of C^{H_2O} using the uptake curve approximation (8). The results show that the difference between the actual and equilibrium water contents never fully disappears even though λ becomes closer to λ_e with increasing γ. We would like to stress here that the curves for $\gamma = 100$ essentially represent the limit at $\gamma \to \infty$ since a further increase of γ does not lead to any discernible variation of the solution.

These results also elucidate the effect of the relaxation parameter on the polarization curve. We found that, at given V_{cell}, the cell current is virtually insensitive to γ. A likely explanation can be seen in Fig. 3b. The modification of the profile of λ, albeit significant, does not lead to substantial change of the total water content, average hydration and, thus, the membrane resistivity.

3.3. Transient regimes

The dynamic response of the cell to a sudden variation of the voltage V_{cell} is illustrated in Fig. 4. The results are obtained by considering step changes in cell voltage from 0.7 to 0.6 V and from 0.6 to 0.7 V. The transient evolution is characterized by very different time scales. The surface overpotential adjusts immediately resulting in an immediate change of current density (Fig. 4a and c). This causes corresponding changes in the concentrations and fluxes of reactants and other gases in the pores of the diffuser and catalyst layers, which occur on the very small diffusive time scale τ_g (about 10^{-3} to 10^{-2} s as estimated in Section 1). Our investigation is focused on the evolution of water and vapor distribution fields. This process is characterized by two larger time scales, that of the water diffusion in the membrane phase and the new time scale τ_γ of the equilibration between the liquid and vapor within the catalyst layer.

The evolution of the average water content of the membrane phase of the catalyst layers in Fig. 4b and d indicates the existence of two time periods. First, lasting about 0.5 s is characterized by relatively fast change of $\langle \lambda \rangle$. Its duration increases with decreasing γ. We can assume that during this period the evolution is dominated by the equilibration between the vapor and liquid water. The second period is much longer and characterized by slow changes of $\langle \lambda \rangle$ both in the catalyst layers and the membrane. This evolution is
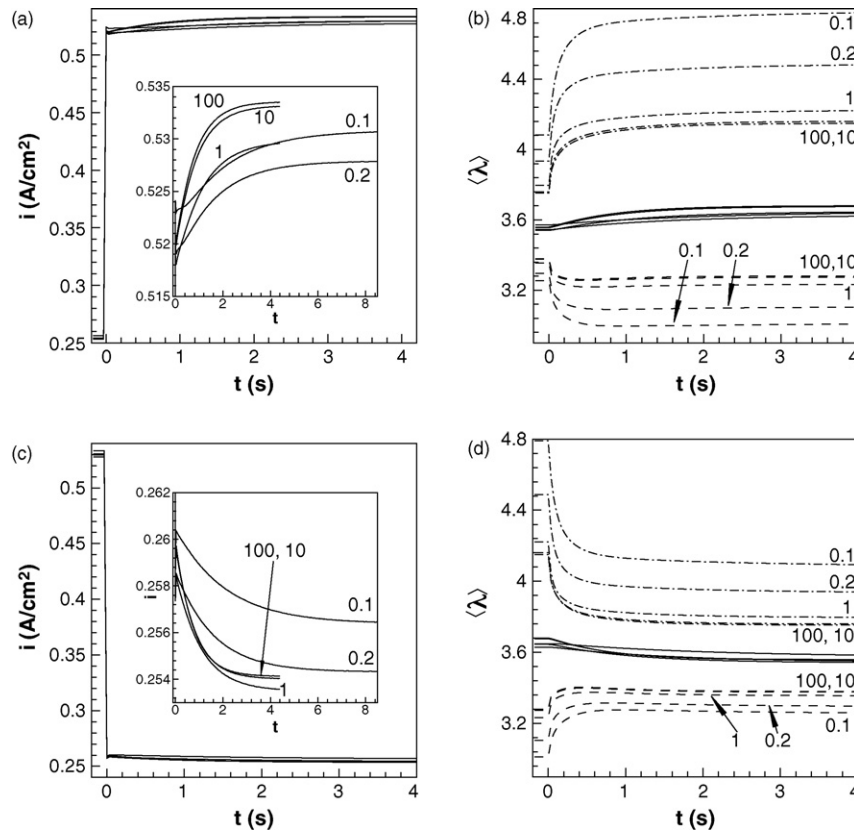
Fig. 4. Dynamic responses to the step change of cell voltage from 0.7 to 0.6 V (a and b) and from 0.6 to 0.7 V (c and d). The external humidity at anode and cathode sides is 50%. (a and c) Current density. (b and d) Average water content of membrane phases of anodic (- - - -) and cathodic (– · –·) catalyst layers, and of the membrane (——). γ varies between 0.1 and 100.

likely to be related to the slow water transport within the membrane.

The variation of the average water content $\langle \lambda \rangle$ in the catalyst layers is rather large especially in comparison with the small variation of the same quantity in the membrane. A further observation can be made that, in agreement with the results obtained for steady-state solutions and illustrated in Fig. 3, the evolution and final asymptotic values of $\langle \lambda \rangle$ in the catalyst layers are significantly affected by the relaxation parameter γ. The difference between the curves for $\gamma = 0.1$ and 100 reaches 10%. On the contrary, the behavior of average water content of the membrane is only weakly sensitive to γ. This translates into the weak sensitivity of the cell current. One can see in Fig. 4a and c that the change of γ can be responsible for a modification in the late stage of the current evolution controlled by the hydration of the membrane and accounting for few percent of the total current variation.

In another simulation experiment, we analyzed the dynamic response of the cell to a change of the humidity conditions. The humidity at the cathode and anode inlet was simultaneously and suddenly changed from 50% to 100%. Such an experiment does not, strictly speaking, represent normal operating conditions, although may occur under special circumstances such as failure of the humidifier. It is also useful since it allows us to investigate the effect of the finite equilibration rate on an unsteady behavior that directly involves change of the membrane water content and vapor concentration of possibly lower amplitude.

A comment is in order regarding the use of the low humidity approximation in the 100% inlet humidity case. It was discussed in Ref. [2] on the basis of earlier calculations that even at currents as high as $1.5\text{A} \times \text{cm}^{-2}$ the level of saturation of liquid water in the cathode diffuser layer does not exceed 5%. At lower currents, such as those considered in the present paper, the saturation is even lower and unlikely to appreciably affect the oxygen transport.

Fig. 5 shows the evolution of the current density i and the average liquid water content $\langle \lambda \rangle$ in the membrane and the catalyst layers. The current density clearly follows the membrane water content in agreement with $\langle \lambda \rangle$ being the main factor of the ionic resistivity. The evolution of the water content can be divided into three stages. During the first very short stage (at the time scale τ_g), the new humidity levels are diffused through the anode and cathode. The dominant phenomenon of the second stage is the phase transition from vapor to ionomer liquid water within the catalyst layers. As a result, the water content of both catalyst layers increases (decreases) sharply as shown in Fig. 5b and d and becomes substantially larger (smaller) than the water content of the membrane. This causes slow diffusion of water through the membrane, which characterizes the third stage of the evolution. The diffusion occurs on the largest time scale of the system. It can be seen in Fig. 5 that the asymptotic steady-state levels of $\langle \lambda \rangle$ are only achieved after about 8 s at $\gamma = 100$ and $\gamma = 10$ and after substantially longer periods at smaller γ.
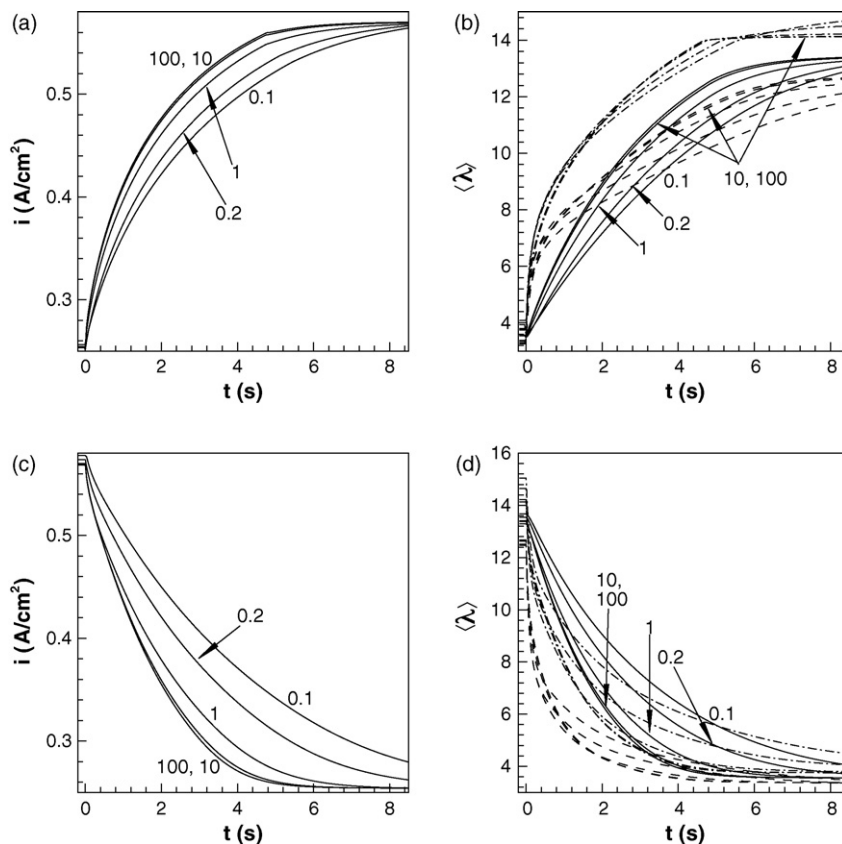
Fig. 5. Dynamic responses to the step change of cathode and anode inlet humidity from 50% to 100% (a and b) and from 100% to 50% (c and d), under $V_{cell} = 0.7$ V. (a and c) Current density. (b and d) Average water content of membrane phases of (- - - -) and cathodic (– · –··) catalyst layers, and of the membrane (——). γ varies between 0.1 and 100.

Second and third stages overlap, which does not allow us to clearly identify the duration of the second stage and hinders the evaluation of the effect of the equilibration parameter γ. The effect is, however, more significant than the case of the transient behavior caused by the voltage change. Lower γ delays the evolution of the membrane hydration and, thus, of the electric current. One can see in Fig. 5a and c that the variation of i with γ, albeit small at the final asymptotic states, is comparably large (up to 25%) during the transient phase, which lasts few seconds.

4. Concluding remarks

This paper presents a one-dimensional isothermal model of a low-humidity non-steady operation of a PEM fuel cell. The main novelty and advantage of the model in comparison with similar existing models is that it does not rely on the non-physical assumption of the uptake curve equilibrium between the pore vapor and ionomer water in the catalyst layers. Instead, the transition between the two phases is modeled as a finite-rate equilibration process. This introduces the typical equilibration time as the third governing time scale of the problem in addition to the typical times of the pore gas diffusion and membrane water diffusion.

A linear model is used to represent the equilibration process. The rate of equilibration is determined by the phenomenological parameter γ, which has the physical meaning of the

non-dimensional reciprocal equilibration time τ_γ. The equilibration time is determined by the typical size of the ionomer water clusters in the catalyst layer and is likely to be of the order of 10^{-4} to 10^{-2} s. Since no reliable experimental data are available for the size of the clusters, we chose to vary γ in a range between 0.1 and 100 corresponding to the equilibration time $8.8 \times 10^{-5} \leq \tau_\gamma \leq 8.8 \times 10^{-2}$ s and conduct a parametric study of the effect of γ on steady-state and transient behavior of the cell.

The study shows that the equilibrium between the vapor and liquid water is never fully achieved within the catalyst layers. Even in the asymptotic limit of fast equilibration, which is represented by the case $\gamma = 100$ in this study, the liquid water distribution is noticeably distinct from the equilibrium distribution given by the uptake curve relation. This is true for both steady-state and transient situations.

The steady-state solutions are found to be affected by the value of γ. The effect on the distributions of liquid water content within the catalyst layers and the membrane is particularly strong. However, this does not lead to comparably noticeable variation of the cell current. This may be explained by considering that the average water content and, thus, the total resistance of the membrane do not change significantly. Another interesting feature of the steady-state solutions is the boundary layer-like behavior of the liquid water content near the surfaces separating the membrane and catalyst layers.

The study also investigates the transient response of a fuel cell to a sudden change of the voltage or external humidity conditions. It is found that the finite-rate equilibration between the catalyst vapor and liquid water can be a significant factor in understanding the internal behavior of the cell. Most importantly, it results in appearance of the additional stage of the response characterized by rapid change of $\langle \lambda \rangle$ within the catalyst layers. This stage precedes and influences the change of the membrane hydration. Its duration is of the order of τ_γ, which implies significant impact of the equilibration parameter on the internal cell evolution. The fact that no appreciable variation of the cell current with γ is found in our simulations does not exclude such a possibility in situations with different operational conditions and/or different set of physical features included in the model.

To conclude, the parametric study presented in this paper shows the importance of the finite rate equilibration within the catalyst layers for the processes of water transport in PEM fuel cells. It is highly desirable to incorporate this phenomenon into the models of cell behavior in order to gain fundamental understanding of transport processes within the cell. However, since the finite-time equilibration does not have any significant effect on cell current, the inclusion of this effect may not be necessary for zero-dimensional models designed to predict the overall performance of a cell. Further investigations are needed, especially those directed toward providing an accurate estimate of the equilibration rate.

References

[1] A.Z. Weber, J. Newman, Chem. Rev. 104 (2004) 4679–4726.
[2] C.-Y. Wang, Chem. Rev. 104 (2004) 4727–4766.
[3] J. Cao, N. Djilali, Canadien Hydrogen Conference, Quebec City, May 2000, pp. 447–456.
[4] P. Futerko, I.-M. Hsing, Electrochim. Acta 45 (2000) 1741–1751.
[5] V. Gurau, H. Liu, S. Kakac, AIChE J. 44 (11) (1998) 2410–2422.
[6] P. Berg, A. Novruzi, K. Promislow, Chem. Eng. Sci. 61 (2006) 4316–4331.
[7] T.E. Springer, T.A. Zawodzinski, S. Gottesfeld, J. Electrochem. Soc. 138 (8) (1991) 2334–2342.
[8] S. Um, C.-Y. Wang, J. Power Sources 156 (2006) 211–223.
[9] F.N. Buchi, S. Srinivasan, J. Electrochem. Soc. 144 (8) (1997) 2767–2772.
[10] Y. Wang, C.-Y. Wang, Electrochim. Acta 50 (2005) 1307–1315.
[11] Y. Wang, C.-Y. Wang, J. Electrochem. Soc. 152 (2) (2005) A445–A453.
[12] T.A. Zawodzinski, J. Davey, J. Valerio, S. Fottesfeld, Electrochim. Acta 40 (3) (1995) 297–302.
[13] F.N. Buchi, G.G. Scherer, J. Electrochem. Soc. 148 (3) (2001) A183–A188.